AN APPROACH TO MAGNETICALLY ACTUATED MINIATURIZED COMPLIANT LOCOMOTION SYSTEMS

T. Kaufhold, V. Böhm, I. Zeidis, K. Zimmermann

Technische Universität Ilmenau, Department of Mechanical Engineering, Technical Mechanics Group, Ilmenau, D-98693, phone: +49-3677-69-2474, fax: +49-3677-69-1823

ABSTRACT

This paper describes two biologically inspired locomotion systems. The first system implements the main advantages of amoeboid movement and is able to move in the plane. The second one is an advanced version of the first system. It uses a magneto-sensitive-elastomeric structure in combination with a periodic magnetic actuation and is vibration driven. Furthermore, an asymmetric configuration of the body is used to generate planar locomotion. The working principle of this system is discussed with the help of modal, transient dynamic and magneto static analyses. Based on the numerical simulations, a prototype was developed, built and verified with experimental tests. Also further results of magneto static analyses and investigations on the first system are presented.

Index Terms **–** compliant locomotion system, vibration driven, mobile robot, magnetic actuation

1. INTRODUCTION

A lot of conventional terrestrial locomotion systems have disadvantages like a restricted mobility and a complex assembly because of the use of conventional actuation principles [1]. The resulting problems are that they have a limited field of application and that they are difficult to miniaturize. Therefore, future robots with high mobility require the use of new, non-conventional locomotion principles. Because of deficits of motion in difficult terrains, the investigation of amoeboid locomotion is of special interest and importance for developing mobile robots.
The movement of the amoeba is characterized by cytoplasmic streaming and continuous changing the body shape [2]-[4]. For an engineer this principle of locomotion offers a fascinating characteristic: the possibility to combine the function of locomotion and manipulation for systems operating in difficult terrains [5].
From the technical point of view the most relevant advantage of amoeboid locomotion is due to the large shape variability. The primary target of known developments is the adaptation of this property. In the biological model shape variability is based on an intrinsic mechanical compliance. The implementation of this property in technical systems is also advantageous, because it allows simple constructions. Further important features are: the locomotion is induced by a single drive mechanism and the direction of locomotion is defined by a local change of the mechanical compliance [6].
Our intention is not a replica of the amoeba, but the adaptation of selected main properties which seem to be advantageous for new locomotion systems with high mobility. Under this condition, the planar miniaturized locomotion system which was initially introduced in [7] was subjected to further investigations in the present contribution. Therefore, a second system with an even simpler assembly and an adjusted actuation principle was developed and built based on this system. In addition, comparative considerations were performed.
The paper begins by providing the design of the locomotion system in Section II and a theoretical explanation of the working principle in Section III, followed by experimental results in Section IV. Finally, in Section V conclusions and future development directions are considered.

2. DESIGN OF THE LOCOMOTION SYSTEM

The use of electroactive polymers (EAP), shape memory alloys (SMA) [8]-[10] or ionic polymer-metal composites (IPMC) [11]-[12] as actuators for miniaturized locomotion systems is common, as

well as pneumatic/hydraulic drives. The disadvantages of these systems are the partly large time constants and the requirement of large numbers of actuators. Alternatively, the implementation of magnetic-based actuators in combination with elastomeric materials offers new actuation possibilities for robotic applications [13]-[14] as well as amoeboid locomotion systems [7]. In addition, the use of magneto-sensitive elastomeric materials (MSE) offers the possibility of simple drive mechanisms [15]. The combination of elastomeric materials (magneto-sensitive or pure elastomeric) with a magnetic actuation allows higher actuation forces as well as an increased deformation range while the response time is being reduced. Robots based on this principle are actuated by shifting elastomeric structure parts with integrated or in case of a MSE without integrated permanent magnets, resulting from a magnetic force. The fast response time of this actuation principle enables the realization of vibration driven systems based on periodic (symmetric/asymmetric) motion of internal masses (symmetric/asymmetric).

Our goal is the realization of planar locomotion systems with a simple assembly. Therefore, the shape variability of the first system is realized by a compliant elastomeric structure, which is divided into three segments with embedded permanent magnets in each segment, see [7]. The second system uses a compliant magneto-sensitive elastomeric structure without integrated permanent magnets. The MSE structure is magnetically actuated by a rotary actuator including three magnets, allowing their periodical deformation. The geometry of the system is based on an equilateral triangle. Fig. 1 illustrates basic configuration and actuating mechanism of the robot.

Due to the 3 axes of symmetry the system is able to form large symmetrical systems (combination of 3, 6, 10… systems by connection of selected corner points, Fig. 13). These systems enable advanced manipulation tasks, such as enclosing and subsequent transport of objects.

In contrast to the first system the resulting magnetic forces between the magnets, housed on the rotor, and the compliant MSE structure are only attractive since the structure only passively react to a magnetic field and not actively operates as an actuator. The magnets on the rotor are oriented in such way that they have the same polarization along the radius (Fig. 1).

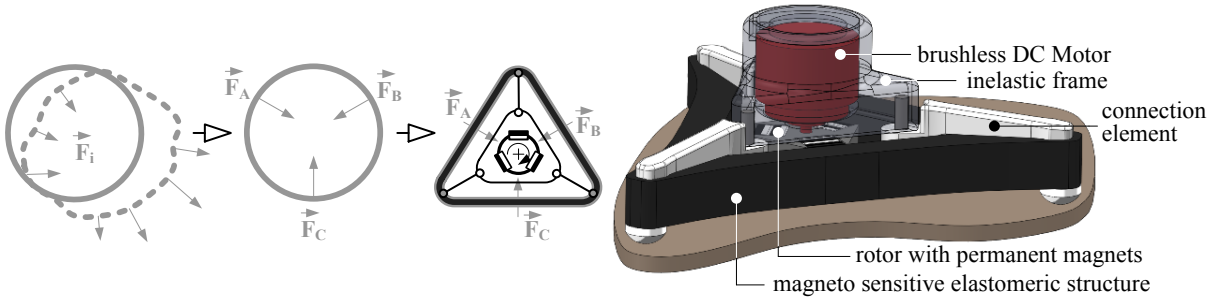

Fig. 1. Left: modelling, steps of abstraction. Right: basic configuration of the second locomotion system.

The locomotion direction of the first system is defined by the asymmetric mechanical compliance of the elastomeric structure. The mechanical compliance of the three segments of the elastomeric structure can be reversibly changed from a compliant to a stiff state. Therefore the “jamming effect” is used, by which a transition between a liquid-like and a solid-like state of granular materials occurs by applying a vacuum [16]-[19].

In contrast to the first system, the second system uses an asymmetric geometry of the compliant MSE structure to generate locomotion in the plane in combination with the magnetic actuation principle. The advantage of this principle is due to the simpler design and easier control while maintaining mobility.

3. THEORETICAL CONSIDERATIONS

3.1 Modeling aspects

Due to the mechanical compliance of both prototypes, the modes of vibration are complex and the locomotion performance of the systems is highly dependent on the driving frequency. To analyze this specific behavior we focus on the description of the mechanical point of view. According to the specific task, geometric nonlinear transient structural finite element analyses were carried out with the

software package ANSYS v12.1. A detailed description of the fundamental method is given in [7]. In this section we focus on the comparison of the two theoretical models of the systems.
The mechanical model of the first system is depicted in Fig. 2. The elastomeric structure of system 1 and the MSE structure of system 2 are modeled with elastic beam elements. For simplicity reasons, masses are concentrated and applied with mass point elements at the nodes of the system. The connections between the beam elements are realized with torsional spring elements. The variable mechanical compliance of the three segments (A, B, and C) of the elastomeric structure is implemented with variable torsional stiffnesses for spring elements at $r=r_1$ (system 1).
In our simplified model, the magnetic forces between the permanent magnets of the rotor and embedded permanent magnets of the elastomeric structure are concentrated and applied on the corresponding mass points of the system (white arrows in Fig. 2).
The mechanical model of the second system is mainly equal to the model of the first system. The differences are:
- there are just attractive forces between the permanent magnets of the rotor and the MSE structure due to the missing outer permanent magnets and the passive characteristics of the structure,
- the mass point at radius r_1 at section C has a mass of m=0.75 g instead of m=1.5 g and
- the torsional spring rate at the position of the adjusted mass was also reduced to model the asymmetry of the magneto-sensitive structure.

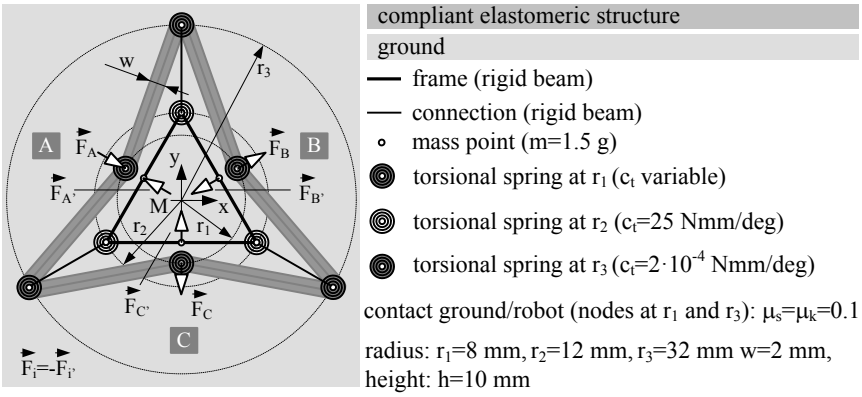

Fig. 2. Mechanical model of the first planar locomotion system (top view, plane of motion: x-y-plane).

Due to a simple model, the movement of the rotor was initially considered with a simple force function as depicted in Fig. 3, with a maximal acting force magnitude of F=0.05 N, and with a variable driving frequency "f". One period of the force function corresponds to one complete rotation of the rotor (periodic time: T=1/f).

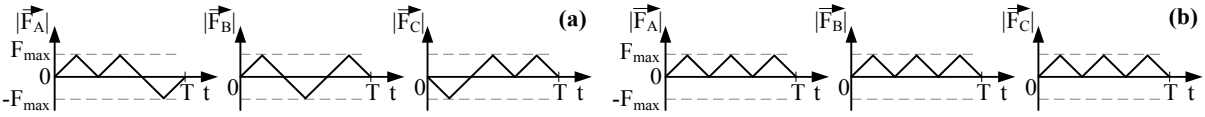

Fig. 3. The applied force functions used in the simulations. (a) system 1, (b) system 2.

3.2 Results of the dynamic simulations
For a first specification of the dynamic system performance, modal analyses, using the Block Lanczos solver, were performed and evaluated, see [7]. For the first system, analyses with a single stiff segment and with two stiff segments were carried out. The calculated natural frequencies differ to each other and are in the lower frequency range because of the significant mechanical compliance of the systems. Two characteristic types of eigenmodes were found: longitudinal oscillations along the symmetry axis with respect to the stiff segment(s) and rotational oscillations around the z-axis (center of rotation: node at $r=r_2$ or r=0).
To describe the movement of the systems dependent on the driving frequency, transient dynamic geometric nonlinear analyses, including all contact conditions and Coulomb-Friction between the elastomeric structure and ground, were carried out, (Fig. 2). In the analyses, the driving frequency of

both systems, the number of stiff segments (1 or 2) of system 1, and the compliance of the segments with variable compliance of system 1 were varied. In the simulations the path of the center of gravity (Point M in Fig. 2), the outer corner nodes and the velocity of both systems were evaluated. Fig. 4 shows selected results of these simulations. Both systems are able to move straight, at a curved path or perform a rotation.

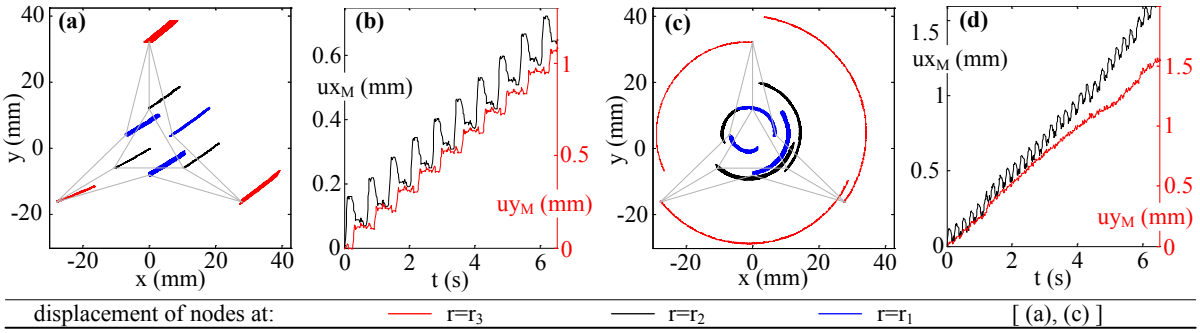

Fig. 4. (a), (c) path of the nodes in the x-y-plane after 100 periods for the driving frequency f=1.5 Hz. (a), (b) first system with two stiff segments. (c), (d) second system. (b), (d): displacement components of the mid-point M (uxM, uyM) in the x-y-plane vs. time for f=1.5 Hz (t=0 s was chosen arbitrarily).

The numerical simulations prove the locomotion of the systems. Furthermore, the locomotion direction and velocity can be changed by varying the driving frequency. As discussed above the goal of the analyses was the quantitative proof of the ability for locomotion of both systems.
Due to the specific magnetic actuation in the following we consider in detail the magneto static behavior of the systems.

3.3 Magneto static simulations

To analyze the resulting magnetic forces of the interacting permanent magnets inside the systems and for a better consideration of the prevailing magnetic forces, magneto static finite element analyses were carried out with the software package ANSYS v13.0.
To calibrate the simulation the magnetic field strength of one permanent magnet with the dimensions: 5x5x2 mm³, material: NdFeB, a residual induction of 1.37 T and coercive field strength of 860 kA/m was measured in the plain. These results were compared with the simulation results of a magneto static simulation with the material parameters and dimensions of the real permanent magnet. Between the measurement and the simulation a maximum deviation of 6.2 % and an average deviation of 3.7 % was determined.
Fig. 5 shows the magnetic model of the first system. The permanent magnets on the outer radius have an equal radial polarization. The inner permanent magnets also have a radial polarization but two of them are attractive and one is repulsive oriented in order to the polarization of the outer magnets, like described in [7]. Fig. 5 (b) shows the orientation of the local coordinate systems of the permanent magnets which are used to determine the resulting magnetic forces on each magnet.

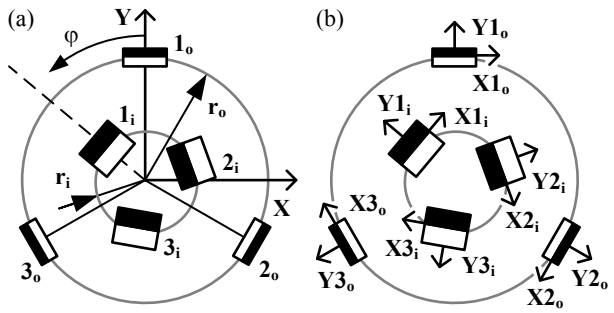

Fig. 5. Scheme of the orientation and polarization (black – north, white – south) of the permanent magnets of prototype 1. (a) X,Y – global coordinate system, 1_i-3_i – inner permanent magnets at radius r_i, 1_o-3_o – outer permanent magnets at radius r_o, φ – rotation angle of the inner permanent magnets. (b) orientation of the local coordinate systems.

Because of different polarizations of the inner magnets the magnetic fields interfere with each other in such way, that the magnetic forces between the inner magnets are not equal.
Several magneto static simulations were performed with different values of the rotation angle and radius of the outer magnets. Selected results of the magnetic flux density at different rotation angles and a fixed outer radius of
r_o=12.9 mm are shown in Fig. 6. The components of the resulting magnetic forces on the outer magnets at five different radiuses r_o and a full rotation of 360 degree are shown in Fig. 7. The components of the magnetic forces achieve their maximum at the radius r_o=10.9 mm with FX_o=0.4 N and FY_o=1.0 N.

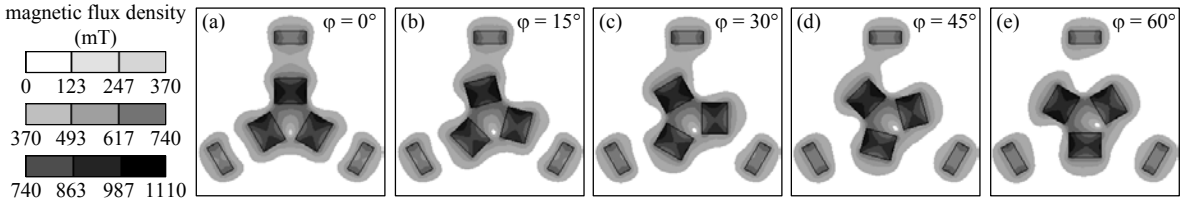

Fig. 6. Simulations of the magnetic flux density at different rotation angles φ and for constant radiuses, r_i=4.3 mm and r_o=12.9 mm, of prototype 1.

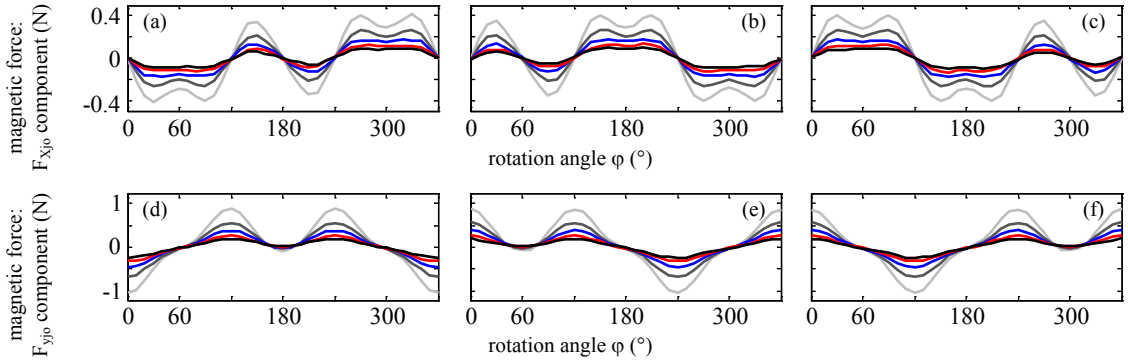

Fig. 7. Components of the magnetic forces (according to their local coordinate systems) of the outer permanent magnets of prototype 1 at different radiuses r_o. (a)-(c) X-component of the magnets 1_o-3_o. (d)-(f) Y-component of the magnets 1_o-3_o. Radius: light grey – 10.9 mm, dark grey – 11.9 mm, blue – 12.9 mm, red – 13.9 mm, black – 14.9 mm. j = 1,2,3.

The absolute value of the magnetic force of permanent magnet 1_i at different distances and a full rotation of 360 degree is shown in Fig. 8. The high magnetic force compared to the forces of the outer magnets results from the interaction of the magnetic fields of the different oriented inner magnets.

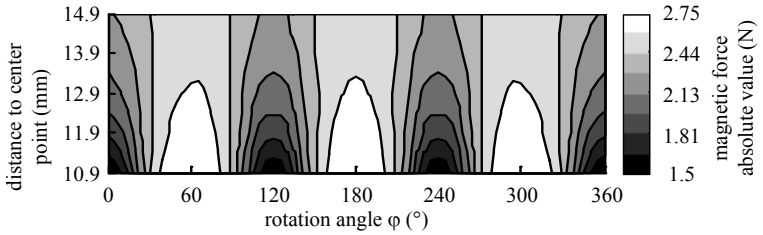

Fig. 8. Absolute value of the magnetic force of permanent magnet 1i at different distances and a rotation of 360 degree.

For prototype two, also a magnetic model was built and magneto static simulations were performed to compare the two prototypes. Because of the missing outer permanent magnets the magnetic flux density has small values in the MSE structure, Fig. 9. Furthermore, the asymmetric geometry has an influence of the magnetic flux density and the resulting magnetic forces. The absolute value of the magnetic force which acts on the segment with the width I=4.5 mm, is 2.47 N while the force acting on the segments with the width II=III=5 mm is 2.53 N.

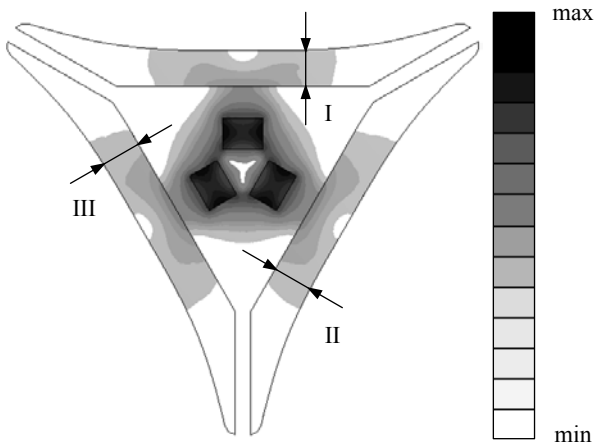

Fig. 9. Simulation of the magnetic flux density of prototype 2. Rotation angle φ=0°. I=4.5 mm, II=III=5 mm.

4. EXPERIMENTAL EVALUATION

Based on the previous modal and transient dynamic geometric nonlinear analyses prototype 1 was developed and built [7]. Based on these results, the magneto static analyses and the transient dynamic geometric nonlinear analyses, prototype 2 was constructed.
Both prototypes differ mainly in the assembly of the elastomeric body and the actuation elements. Fig. 10 shows the CAD models of the prototypes in an exploded view.

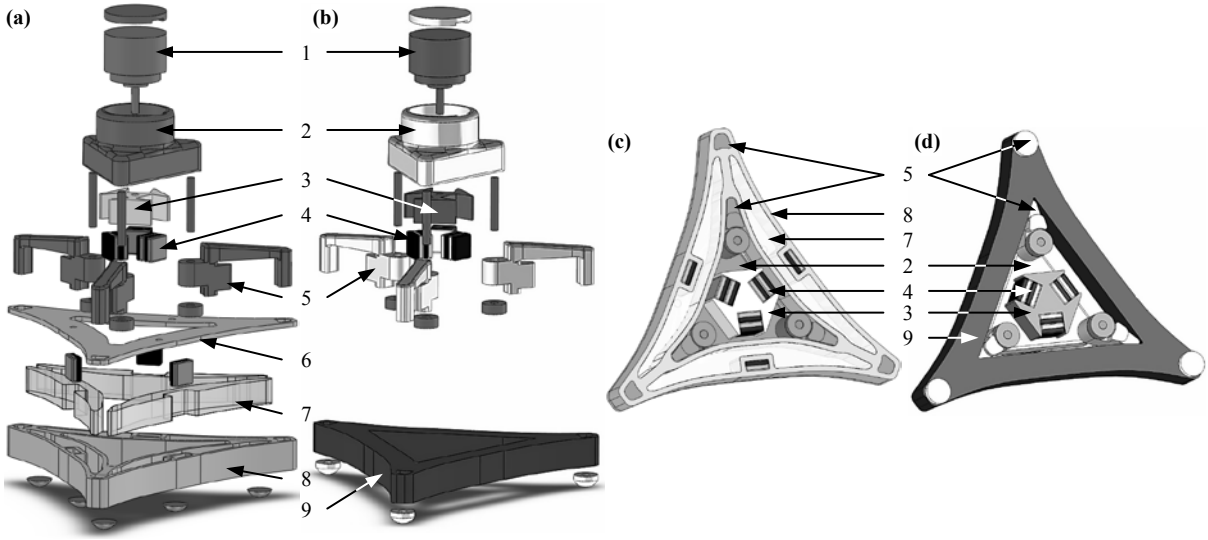

Fig. 10. Exploded view of the prototypes: 1 (a) and 2 (b). (c) and (d): bottom view of the prototypes with silicone elastomer body cut open (c); 1- motor, 2- housing, 3- rotor, 4- magnets, 5- plastic skeleton, 6- elastomer body top, 7- glass particles, 8- elastomer body bottom, 9- magneto-sensitive elastomer).

As assumed in the simulations, the first system is based on a periodic asymmetric deformation of a compliant body and the second system is based on the periodic deformation of an asymmetric compliant body. In both prototypes the periodic deformation is magnetically induced only by one central rotary drive. The locomotion direction of prototype 1 can be defined by changing the mechanical compliance of selected segments of the elastomeric structure using the jamming effect as discussed in [7]. Prototype two is able to change the direction of locomotion by varying the output speed of the motor.
The developed prototypes are driven by a single brushless DC-Gearmotor ("penny-motor technology" series 1309 004 BH, mass: 2.8 g, diameter: 12.5 mm, height: 10.8 mm) with a torque of 5 Nmm (continuous operation) at an output speed of 111 rpm. The motor is driven by a speed controller (Faulhaber speed controller series SC 1801) which has a PWM signal output with a nominal voltage

UN=4 V. Attached to the shaft of the motor are six permanent magnets (material: NdFeB, dimensions: 5x5x2 mm³, residual induction 1.37 T) in pairs of two.
The compliant body of prototype 1 (Fig. 10 (a) and (c), Prototype: diameter: 67.5 mm, height: 21.5 mm, total mass: 19.4 g) has a mass of 4.6 g and is made of condensation-curing silicone elastomer (shore hardness: A8) and is divided into three chambers which are filled with spherical glass particles (diameter: 150-210 µm, filling factor: 60 %). The chambers have hose connections (outer diameter: 1 mm, inner diameter: 0.5 mm, material: PVC) by which the compliance of the segments of the elastomeric structure can be locally changed when evacuating the air. Moreover, permanent magnets are installed in the middle of each side.
The magneto-sensitive elastomer body of prototype 2 (Fig. 10 (b) and (d), Prototype: diameter: 67.5 mm, height: 23 mm, total mass: 21.6 g) has a mass of 12.7 g and is made of addition-curing silicone elastomer (shore hardness: A8). The mass ratio of the silicone elastomer and carbonyl iron particles (particle size 6 µm) is 3:1. The particles were added to the silicone elastomer during the manufacturing process and the composite was vulcanized in absence of a magnetic field.
In both prototypes the motor is enclosed by, and the silicone elastomer body is attached to a plastic material skeleton (ABS-Copolymer, density: 1.04 g/cm3) manufactured with rapid prototyping. Between the prototypes and the ground, the measured coefficient of static friction is μ_0=0.15 and the coefficient of kinetic friction is μ=0.077.
The following motion analyses of the prototypes were recorded with a high-speed camera (model: HCC-1000; manufacturer: Vosskühler GmbH; recording parameter: 31.83 FPS). To compare the flexibility of both systems the housing was fixed and the motion of the elastomeric bodies was recorded at a motor speed of 133 rpm. The videos were analyzed using Matlab R2011a performing a contour detection using image transformations and morphological operations to detect the outer outline. Selected results are shown in Fig. 11 (b) – (d),(f). The second system shows a high flexibility and higher bending angles. This experiment also proves the effectiveness of the jamming-effect for changing the mechanical compliance of the segments of prototype 1.

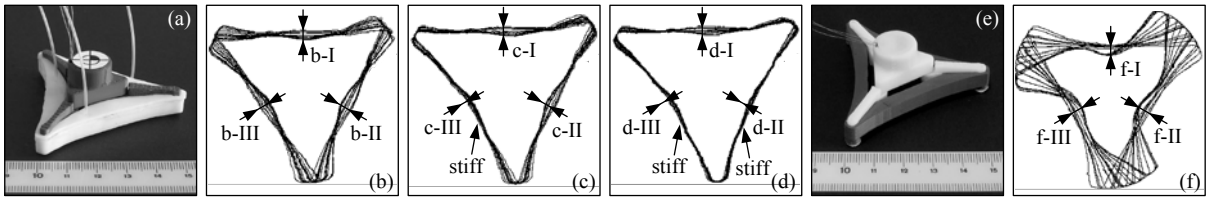

Fig. 11. (a), (e) Snapshots of the assembled prototypes: 1 (a) and 2 (e). (b)-(d) Motion range of prototype 1 with fixed housing and no stiff segment (b), one stiff segment (c), two stiff segments (d), b-I=3.2 mm, b-II=b-III=4mm, c-I=3.2 mm, c-II=2.7 mm, c-III=2 mm, d-I=2.8 mm, d-II=d-III=1.7 mm. (f) Motion range of prototype 2 with fixed housing, f-I=4.1 mm, f-II=f-III=5.1 mm.

Furthermore, the locomotion of the prototypes was recorded. These videos also were analyzed and the movement of the mid-point evaluated, see Fig 12. Selected results of prototype 1 ([6], [7] in Fig. 12) were determined with the actuation parameters: 167 rpm output speed of the motor (direction: clockwise) and 97% vacuum connected to the chambers (two stiff segments Fig. 12 [I], [6] and one stiff segment Fig. 12 [II], [7]). Selected results of the second system at five different output speeds of the motor (direction: clockwise) are also depicted in Fig. 12 [1]-[5].
The experiments have shown that locomotion in the plain is possible with both prototypes. In accordance with the theoretical analyses, the velocity as well as the locomotion direction of system 1 depends on the magnitude of the vacuum, on the number of depressurized chambers, and on the speed of the motor. As assumed in the theoretical considerations the locomotion direction and velocity of prototype 2 depends on the output speed of the motor.
The determined maximum average speeds for the prototypes are: 2.17 mm/s (prototype 1, two stiff segments) and 6.54 mm/s (prototype 2 at 150 rpm). The experiments have shown a direct connection of the driving frequency and the movement of prototype 2: The higher the driving frequency of the system, the bigger the curvature of the movement path. This behavior is also confirmed by the numerical simulations.

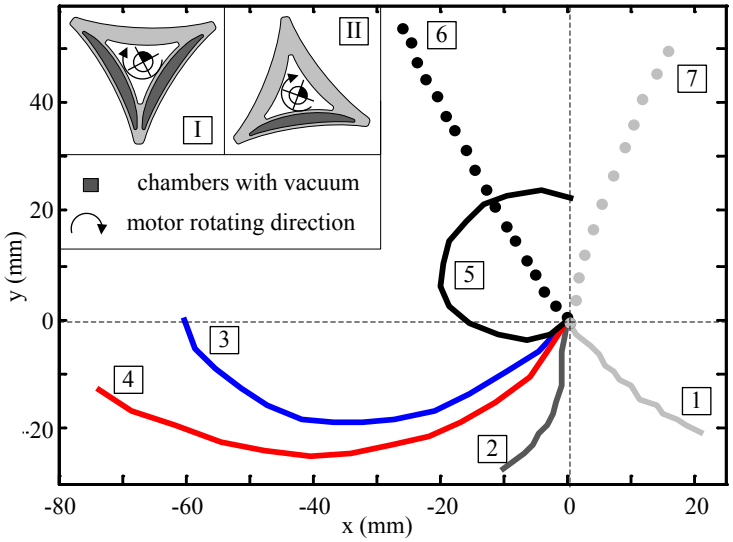

Fig. 12. Motion of the locomotion systems. Mid-point displacement analyzed and depicted.
[6]-[7]: prototype 1 with two ([I], [6]: black-dotted) and one ([II], [7]: grey-dotted) stiff segments. Time interval 27 s. [1]-[5]: prototype 2 at different output speeds of the motor. [1]: light grey – 100 rpm, [2]: dark grey – 117 rpm, [3]: blue – 133 rpm, [4]: red – 150 rpm, [5]: black – 167 rpm. Time interval for all speeds: 13 s.

5. CONCLUSIONS AND FUTURE DEVELOPMENT

This paper presents concepts for vibration-driven miniaturized compliant locomotion systems based on magnetic actuation. Therefore, magneto static and other numerical simulations were performed to examine the locomotion performance of systems based on this principle.
Two prototypes were built and tested. The planar movement of the first system is achieved by an asymmetric periodic deformation of a compliant structure, including segments with variable mechanical compliance. The second system is able to move in the plain due to a varying periodic deformation of an asymmetric compliant structure.
In contrast to the biological object, the level of abstraction of the technical systems is high, resulting from a desired simple design. The main idea by the design of the first system was the biological inspired implementation of the variable mechanical compliance. The local change of the compliance during locomotion is used to change the movement direction. The locomotion performance of the second prototype is better because it is able to move faster than the first system. Furthermore, this system has a simpler assembly and is easier to control. Also, it has a very low energy consumption of 0.65 W which is lower than the consumption of the 1. system because it doesn't need a vacuum pump.
Future work is addressed to increase shape variability of the systems, determine optimal control strategies, and investigations on the behavior of the robots at loose/compliant ground and in liquid media. Moreover, experiments with combined systems are of interest, Fig. 13.
Also we focus on systems with prestressed compliant segments and on fully compliant prestressed structures to increase the movement performance.

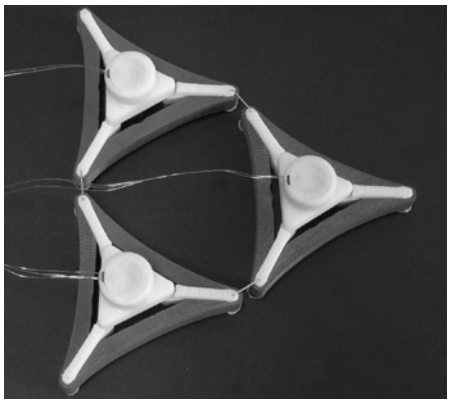

Fig. 13. Combination of three prototypes of system 2.

REFERENCES

[1] K. Zimmermann, I. Zeidis, and C. Behn, Mechanics of Terrestrial Locomotion – With a Focus on Non-pedal Motion Systems, Springer, Berlin, 2009, ch. 6.

[2] S.S. Rogers, Th.A. Waigh, J.R. Lu, "Intracellular microrheology of motile Amoeba proteus," in Biophys. Journal, vol. 94, 2008, pp. 3313-3322.

[3] Th.P Stossel, "On the crawling of animal cells," in Science, vol. 260, 1993, pp. 1086-1094.

[4] J. Condeelis, "Life at the leading edge: formation of cell protrusion," in Annu. Rev. Cell. Biol., vol. 9, 1993, pp. 414-440.

[5] K. Zimmermann, and V. Böhm, "A contribution to the amoeboid locomotion of mobile robots," in Proc. of ISR2010, 41st Int. Symposium on Robotics, München, 2010, pp. 1153-1157.

[6] C. Tropea, and H. Bleckmann (eds.), Nature-Inspired Fluid Mechanics, Springer, Berlin, 2012.

[7] T. Kaufhold, V. Böhm, K. Zimmermann, "Design of a miniaturized locomotion system with variable mechanical compliance based on amoeboid movement" in Proc. of the 4th IEEE RAS & EMBS Int. Conf. on Biomedical Robotics and Biomechatronics (BioRob), Roma, 2012, pp. 1060 – 1065.

[8] A. Menciassi, S. Gorini, G. Pernorio, L. Weiting, F. Valvo, and P. Dario, "Design, Fabrication and Performances of a Biomimetic Robotic Earthworm," in Proc. of 2004 IEEE Int. Conf. on Robotics and Biomimetics, Shenyang, 2004, pp. 274-278.

[9] J.-S. Koh, and K.-J. Cho, "Omegabot: Biomimetic Inchworm Robot Using SMA Coil Actuator and Smart Composite Microstructures (SCM)," in Proc. of 2009 IEEE Int. Conf. on Robotics and Biomimetics, Guilin, 2009, pp. 1154-1159.

[10] S. Seok, C. D. Onal, R. J. Wood, D. Rus, and S. Kim, "Peristaltic locomotion with antagonistic actuators in soft robotics," in Proc. of 2010 IEEE Int. Conf. on Robotics and Automation, Anchorage, 2010, pp. 1228-1233.

[11] B. Kim, D.-H. Kim, J. Jung, and J.-O. Park, "A biomimetic undulatory tadpole robot using ionic polymer–metal composite actuators," in J. Smart Mater. Struct., vol. 14, 2005, pp. 1579–1585.

[12] Z. Chen, S. Shatara, and X. Tan, "Modeling of Biomimetic Robotic Fish Propelled by An Ionic Polymer–Metal Composite Caudal Fin," in IEEE Transactions on Mechatronics, vol. 15, no. 3, 2010, pp. 448-459.

[13] G. Tortora, S. Caccavaro, P. Valdastri, A. Menciassi, and P. Dario, "Design of an autonomous swimming miniature robot based on a novel concept of magnetic actuation," in Proc. of 2010 IEEE Int. Conf. on Robotics and Automation, Anchorage, 2010, pp. 1592-1597.

[14] S. H. Kim, S. Hashi, and K. Ishiyama, "Methodology of Dynamic Actuation for Flexible Magnetic Actuator and Biomimetic Robotics Application," in IEEE Transactions on Magnetics, vol. 46, no. 6, (2010), pp. 1366-1369.

[15] K. Zimmermann, V. Böhm, I. Zeidis, "Vibration-driven mobile robots based on magneto-sensitive elastomers," in Proc. of the IEEE/ASME Int. Conf. on Intelligent Advanced Mechatronics, Budapest, 2011, pp. 730-735.

[16] E. Steltz, A. Mozeika, N. Rodenberg, E. Brown, H.M. Jaeger, "JSEL - Jamming Skin Enabled Locomotion," in Proc. of the IEEE/RSJ Int. Conf. on Int. Robots and Systems, St. Louis, 2009, pp. 5672-5677.

[17] A. Liu, S. Nagel, "Jamming is not just cool anymore," in Nature, vol. 396, 1998, pp. 21.

[18] E. Steltz, A. Mozeika, J. Rembisz, N. Corson, and H.M. Jaeger, "Jamming as an Enabling Technology for Soft Robotics," in Electroactive Polymer Actuators and Devices (EAPAD) 2010, ed. Yoseph Bar-Cohen, Proc. SPIE vol. 7642 (Conference on Smart Structures/NDE 2010, March 7-11, 2010, San Diego).

[19] E. Brown, N. Rodenberg, J. Amend, A. Mozeika, E. Steltz, M. R. Zakin, H. Lipson, and H. M. Jaeger, "Universal Robotic Gripper based on the Jamming of Granular Material," in Proc. National Academy of Sciences, vol. 107, no. 44, 2010, pp. 18809-18814.

ACKNOWLEDGMENTS

This work was supported by DFG as part of priority program 1681 grant ZI 540-17/1.

CONTACTS

M.Sc. T. Kaufhold tobias.kaufhold@tu-ilmenau.de
Dr.-Ing. V. Böhm valter.boehm@tu-ilmenau.de
Dr. rer. nat. I. Zeidis igor.zeidis@tu-ilmenau.de
Univ.-Prof. Dr.-Ing. habil. K. Zimmermann klaus.zimmermann@tu-ilmenau.de

